Nonlinear dynamics of cooperative upconversion

P. Xie* and S. C. Rand

Division of Applied Physics, 1049 Randall Laboratory, University of Michigan, Ann Arbor, Michigan 48109-1120

Received July 15, 1993; revised manuscript received November 29, 1993

We describe several new aspects of light–matter interactions for solids in which interatomic coupling of impurity atoms plays a dominant role in population dynamics. We explore the implications of spatial coherence in such multiatom interactions by introducing a density-matrix theory of cooperative upconversion, focusing on pair systems for which analytic results can be obtained. We predict population pulsations in coherent cooperative upconversion, enhanced quantum efficiency, enhanced energy transfer, and pair-mediated instabilities, not only in cooperative upconversion media without external cavities but in upconversion lasers and conventional lasers in highly doped solids as well. These predictions are compared with rate equation solutions and observations in lasers with inversions sustained by cooperative processes, particularly the 2.8-μm Er laser. Rate equations fail to predict the observed steady-state instabilities of this laser, which are well reproduced by density-matrix theory, furnishing evidence of weak coherent delocalizations in a rare-earth system.

1. INTRODUCTION

Upconversion and energy-transfer processes that occur in solids as a result of nonlinear population dynamics, rather than parametric processes, have been studied for many decades.[1–3] Two classes of nonparametric upconversion that differ in the mechanism responsible for converting long-wavelength radiation incident upon a sample into short-wavelength emission are generally acknowledged. In the first, sequential absorption of incident photons by progressively higher energy levels of a single atom leads to emission from high-lying upconverted states, broadly designated as upconversion emission. In the second, each atom absorbs at most one photon, and energy transfer between atoms is required for upconversion emission. The latter type of process may proceed in one of three ways. In a cooperative process the pooled energy of several coupled atoms can become localized on one particular atom, which then emits light from a high-lying, upconverted state.[3] Or energy may be transferred in a sequence of discrete transfer steps.[1] Another possibility is an avalanche process in which upconversion results from field-induced cross-relaxation dynamics.[4,5] In this paper we confine our discussion to the cooperative upconversion process, highlighting novel experimental and theoretical dynamics that can result from spatial coherence among the coupled atoms or from the interaction of coupled atoms with radiation fields in optical cavities.

Early research on upconversion was motivated by the need to overcome the poor sensitivity of infrared detectors.[6] More recent research on upconversion has been stimulated by the realization that upconversion lasers have potential as practical, solid-state sources of visible and ultraviolet light.[7–13] However, to date, little discussion has been given to certain fundamental aspects of the upconversion processes themselves, such as basic limits to achievable degrees of upconversion and the inherent stability of these highly nonlinear interactions between light and matter.

In this paper we consider these topics, primarily in the context of new experiments with the pair-pumped Er laser, a laser with an inversion sustained purely by pair upconversion.[14] General predictions of enhanced quantum efficiency, enhanced energy transfer, population pulsations, and instabilities mediated by cooperative dynamics are compared with observations of nonlinear dynamics in twofold, threefold, and fourfold upconversion processes.

2. THEORY

A. Enhanced Quantum Efficiency

The general scheme of cooperative upconversion is illustrated in Fig. 1. Two atoms are depicted in an excited state undergoing a pair transition in which one atom is promoted to an upper state while the other descends to the ground state. Multipole or exchange coupling is presumed to furnish the interaction responsible for this pair transition, mediating evolution of the system in a manner somewhat analogous to coupled harmonic-oscillator dynamics. The energy transferred to the second atom rarely matches the precise transition energy required for gaining access to a real final state, but the energy defect can be accommodated in solids by the emission or the absorption of phonons. In solids doped heavily with rare earth or transition-metal impurities, transitions of this kind are common.[2]

A schematic representation of excitation and decay pathways involved in cooperative upconversion is given in Fig. 2. Excitation is initiated by a pumping process at wavelength λ_{in}, which populates level $|3\rangle$ with efficiency η_0. The system subsequently cascades to level $|1\rangle$ in steps with individual branching ratios η_i. Decay to the ground state $|0\rangle$ may then occur, or a cooperative transition of the type indicated in Fig. 1 may take place. The manner in which cooperative upconversion benefits the overall emission at λ_{out} is not immediately obvious because the maximum branching ratio for a single pair upconversion process is 0.5. This seems low from the outset. However, it can readily be appreciated from

0740-3224/94/050901-13$06.00

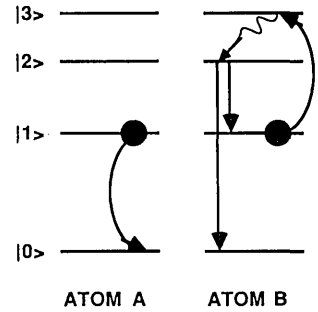

Fig. 1. Dynamics of cooperative upconversion in a system consisting of two four-level atoms initially occupying state $|1\rangle$, as indicated by filled circles. The system relaxes by promoting one atom to level $|3\rangle$ as the second decays to the ground state (curved arrows). In this fashion upconversion fluorescence from energy levels higher than the initial state becomes possible at several wavelengths (straight arrows). The correspondence between levels of the model and Er is as follows: $|0\rangle \leftrightarrow {}^4|_{15/2}$, $|1\rangle \leftrightarrow {}^4|_{13/2}$, $|2\rangle \leftrightarrow {}^4|_{11/2}$, $|3\rangle \leftrightarrow {}^4|F_{9/2}$.

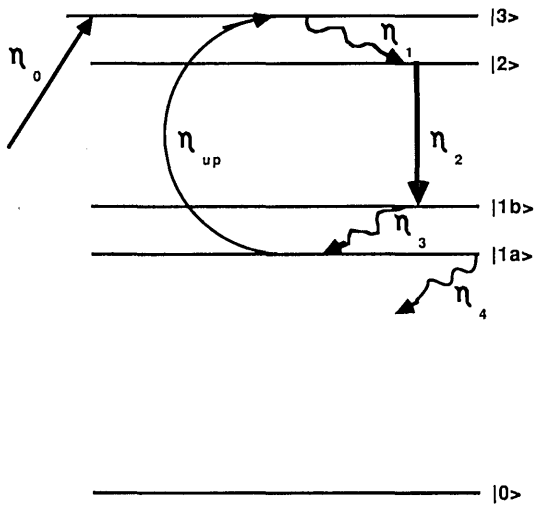

Fig. 2. Recycling by cooperative upconversion. The initial excitation of level $|3\rangle$, either by resonant optical excitation or by a cooperative process, occurs with quantum efficiency η_0. This is followed by a cascade of nonradiative decay and emission processes with individual branching ratios of η_i. States $|1a\rangle$ and $|1b\rangle$ are different Stark components of level $|1\rangle$. Finally a long-lived level is reached in which cooperative upconversion can occur spontaneously without further absorption of photons from the pump field. The remnant excited-state population can be recycled to level $|3\rangle$ and additional photons may be emitted, thereby enhancing quantum efficiency. The radiative transition $|2\rangle \rightarrow |1b\rangle$ is the focus of quantum-efficiency considerations.

Fig. 2 that excited-state population can be recycled through the emission channel if spontaneous upconversion occurs.

To quantify this concept and to show that quantum efficiency of optical emission can be enhanced by the presence of cooperative dynamics, we assume that the cooperative upconversion process can repeat itself n times. The number of sites at which upconversion occurs is taken to be small compared with the number of excited atoms. This ensures that the reservoir of state $|1\rangle$ ions surrounding upconversion sites remains undepleted through many upconversion cycles because of rapid energy migration within the reservoir. Ground-state A atoms at upconversion sites are continually reexcited to state $|1\rangle$ by means of resonant energy transfer from the reservoir, restoring the initial condition shown in Fig. 1 without requiring the absorption of additional photons. For very large n the effective quantum efficiency then becomes

$$\begin{aligned}\eta_{\text{eff}} &= \eta_0\eta_1\eta_2[1 + \eta_3\eta_{\text{up}}P^{(1)}\eta_1\eta_2 \\ &\quad + \eta_3\eta_{\text{up}}P^{(1)}\eta_1\eta_2\eta_3\eta_{\text{up}}P^{(2)}\eta_1\eta_2 + \cdots] \\ &= \sum_{n=0}^{\infty}\eta_0\eta_1\eta_2(\eta_3\eta_{\text{up}}\eta_1\eta_2)^n = \frac{\eta_0\eta_1\eta_2}{1 - \eta_1\eta_2\eta_3\eta_{\text{up}}}. \quad (1)\end{aligned}$$

Here factors $P^{(n)}$ are introduced to account explicitly for the probability of A's being reexcited by energy migration during the nth cycle. Both atoms A and B must be in state $|1\rangle$ for upconversion to occur with branching ratio η_{up}. However, $P^{(n)}$ may be set equal to unity without a significant loss of generality [$P^{(1)} = P^{(2)} = \ldots P^{(n)} = 1$]. For a fixed initial number of excited atoms, $P^{(n)}$ decreases as the reservoir depletes, but it is an excellent approximation to assume that $P^{(n)}$ is independent of n when the density of upconversion sites is low compared with the density of excited atoms, and steady-state illumination is assumed. We can compare the effective efficiency η_{eff} with that expected without population recycling by defining an enhancement factor M, given by

$$M = \eta_{\text{eff}}/\eta_0\eta_1\eta_2 = (1 - \eta_1\eta_2\eta_3\eta_{\text{up}})^{-1}. \quad (2)$$

It is immediately apparent from Eq. (2) that quantum efficiencies exceeding unity are possible. To see this, one can ignore decay from the upconversion state $|1a\rangle$ by setting $\eta_4 = 0$ and the value $\eta_{\text{up}} = (1/m) - \eta_4 = 1/m$ into Eq. (2). m is the number of atoms participating in the upconversion process itself. Then, for example, a quantum efficiency of 2 is expected when branching ratios for decay and emission in the system equal unity, and η_{up} is taken to be 0.5, the maximum value appropriate for pair upconversion. This is of great significance because population recycling also yields an enhanced energy conversion efficiency given by

$$\eta_E{}^* = \eta_{\text{eff}} \times \lambda_{\text{in}}/\lambda_{\text{out}}. \quad (3)$$

From Eq. (3) it is clear that, for rates of cooperative upconversion greatly exceeding the natural decay rate of state 2, energy efficiency ceases to depend sensitively on the actual value of the upconversion rate itself or on the upconversion branching ratio and attains an enhanced value.

This result exhibits a universality that holds irrespective of the pumping method. Two examples are instructive. First, if all excitation above level $|1\rangle$ is furnished by m-fold upconversion, one might expect the maximum energy efficiency to be low [$\eta_E = (1/m)\lambda_{\text{in}}/\lambda_{\text{out}}$] because with $\eta_0 = 1/m$ only one in m excited atoms reaches the emitting level. However, with population recycling the maximum upconversion energy efficiency is found from Eqs. (1) and (3) to acquire the enhanced value $\eta_e{}^* = [1/(m - 1)]\lambda_{\text{in}}/\lambda_{\text{out}}$. Because λ_{out} may be as short as $\lambda_{\text{in}}/(m - 1)$ in this case, giving $\lambda_{\text{in}}/\lambda_{\text{out}} \leq (m - 1)$, the energy efficiency can approach unity.

Second, when a short input wavelength is used to pump upper level $|3\rangle$ optically, as in a conventional laser-pumping scheme, cooperative enhancement of quantum

efficiency can still occur, provided that $\lambda_{in}/\lambda_{out} \leq (m-1)/m$, constraining downward and upward transitions to conserve energy in the cooperative process. We again find that the maximum conversion efficiency $(\eta_E{}^*)_{max} = \{m\lambda_{in}/[(m-1)\lambda_{out}]\}_{max} = 1$ exceeds the limiting value set by $(\eta_E)_{max} = (\lambda_{in}/\lambda_{out})_{max} = (m-1)/m$ for the same emission process in the absence of recycling. Energy conversion efficiency $\eta_E{}^*$ never exceeds unity because of the restrictions on $\lambda_{in}/\lambda_{out}$ necessary for energy transfer to occur between excited states.

B. Population Pulsations

Modifications of cooperative dynamics are to be expected in optical cavities. This may happen, for example, if stimulated emission follows cooperative upconversion. For a stimulated emission process that repopulates coupled levels while depleting the gain, a sudden increase in the cooperative upconversion rate follows gain quenching. The abruptly increased rate of upconversion tends to restore inversion, and a relaxation oscillation can take place.

Rate equation calculations indicate that steady relaxation oscillations cannot be sustained by cooperative dynamics, a result considered in more detail in Subsection 2.C. However, transient oscillations can appear during the buildup or the decay of light in the cavity. We may show this by solving the rate equations for populations N_i in each state $(i = 0, 1, \ldots, 3)$ together with the equation for cavity photon density Q:

$$\frac{dN_0}{dt} = \gamma_{30}N_3 + \gamma_{20}N_2 + \gamma_{10}N_1 + \alpha N_1{}^2 - B_{01}I(N_0 - N_1), \tag{4}$$

$$\frac{dN_1}{dt} = \gamma_{31}N_3 + \gamma_{21}N_2 - \gamma_{10}N_1 - 2\alpha N_1{}^2 + B_{01}I(N_0 - N_1) + B_{12}Q(N_2 - N_1), \tag{5}$$

$$\frac{dN_2}{dt} = \gamma_{32}N_3 - \gamma_2 N_2 - B_{12}Q(N_2 - N_1), \tag{6}$$

$$\frac{dN_3}{dt} = -\gamma_3 N_3 + \alpha N_1{}^2, \tag{7}$$

$$\frac{dQ}{dt} = B_{12}Q(N_2 - N_1) - \frac{Q}{\tau_c}. \tag{8}$$

In these expressions γ_{ij} is the decay constant between levels i and j, γ_i is the total decay rate for level i, B_{ij} is the Einstein coefficient for induced absorption on the $i \rightarrow j$ transition, and α is the upconversion coefficient, which has dimensions of volume. I is the intensity of incident light, and τ_c is the cavity lifetime.

To simulate the dynamics in a cavity after illumination stops, the stationary-state populations reached in levels $|0\rangle$ to $|3\rangle$ during constant pumping were obtained. Then we solved the undriven equations for times after pumping ceased by utilizing the stationary-state parameters $Q(0)$ and $N_i(0)$ as initial conditions. The resulting level $|2\rangle$ population dynamics are shown in Fig. 3.

Two aspects of the dynamics calculated with this rate equation approach are interesting. First, for times shorter than the lower-state lifetime but greatly in excess of the cavity lifetime, it is possible for a population inversion to persist between levels $|2\rangle$ and $|1\rangle$ after pumping has stopped. When the net rate of pumping into state $|1\rangle$ drops to zero, the rate of cooperative upconversion that feeds the upper laser level remains nearly constant initially, so the inversion improves for a short time. Second, the optical feedback in a cavity introduces transient atom–field interactions that cannot otherwise take place (see Subsection 2.C). Oscillations, reflecting population pulsations in the upconversion medium, are predicted in the rate equation limit and should be evident in light emitted from the cavity.

In the absence of inversion or a cavity, such population pulsations are possible only in spatially coherent cooperative interactions. To verify this, the role of delocalization in excited states must be examined carefully with a

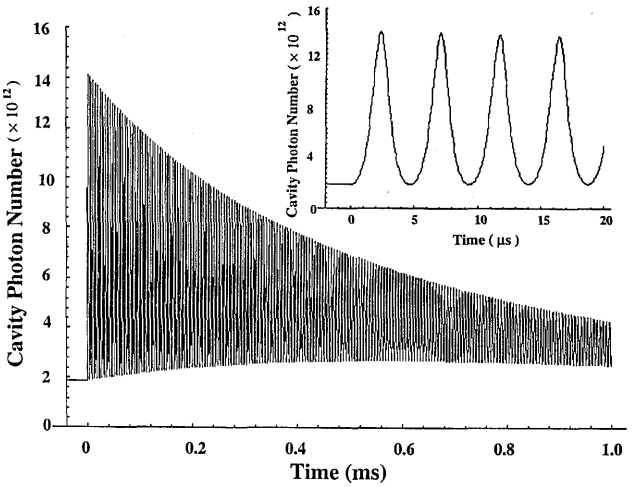

(a)

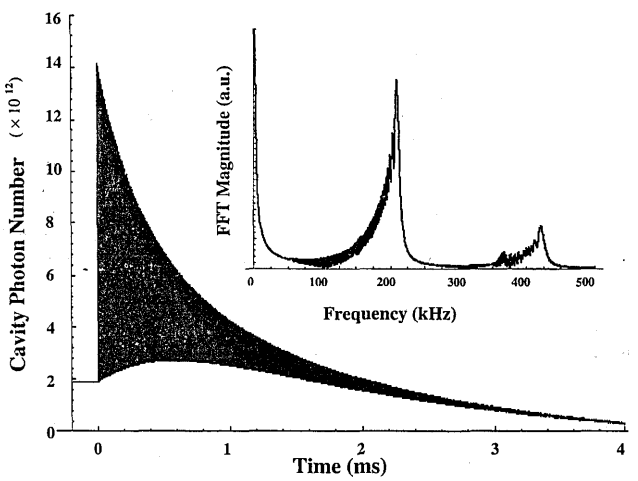

(b)

Fig. 3. Numerical rate equation calculation of pulsations in the inversion of the pair-pumped laser after termination of steady-state excitation. There are no free parameters: intensity $I = 153\ \mathrm{W/cm^2}$ (1.7 times threshold) in a cavity ($\tau_c = 1.5$ ns) of dopant density $5.7 \times 10^{20}\ \mathrm{cm^{-3}}$ with $\gamma_2 = 0.0714\ \mathrm{ms^{-1}}$, $\gamma_3 = 0.179\ \mathrm{ms^{-1}}$, $\gamma_{31} = 0.0769\ \mathrm{ms^{-1}}$, $\gamma_{32} = 0.103\ \mathrm{ms^{-1}}$, $\gamma_4 = 143\ \mathrm{ms^{-1}}$, $B_{01} = 6.9 \times 10^{-2}\ \mathrm{cm^2/J}$, $B_{12} = 2.4 \times 10^{-10}\ \mathrm{cm^3/s}$,[15] and $\alpha = 3.2 \times 10^{-17}\ \mathrm{cm^3/s}$.[16] (a) The initial part of postexcitation decay (inset, magnified trace with temporal resolution on the microsecond time scale showing quasi-periodicity). (b) Postexcitation decay at coarse temporal resolution [inset, fast-Fourier-transform (FFT) spectrum].

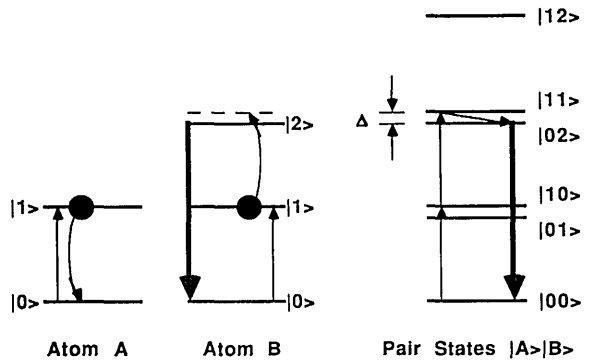

Fig. 4. Energy-level diagram of a model pair system. Left, individual atoms A and B may be pictured as each absorbing one pump photon (thin vertical arrow) to reach the interaction level indicated by the filled circles. Pair upconversion then leads to upconversion fluorescence after accommodation of the energy mismatch Δ, as indicated by the thick vertical arrow. Right, an alternative representation shows the coupled pair system as a ladder of product states $|A\rangle|B\rangle$. Absorption of two pump photons is required for promotion of the pair system to state $|11\rangle$. Direct excitation to state $|02\rangle$ by two-photon absorption of a single atom is off resonant because of the energy defect Δ. Emission from state $|02\rangle$ occurs after spontaneous pair upconversion, which may be viewed as an internal relaxation from state $|11\rangle$ to $|02\rangle$ accompanied by emission of phonons for energy conservation.

different formalism. Although energy transfer is widely treated with rate equations as a one-way, incoherent process between a donor and an acceptor,[3] a density-matrix treatment can be used to incorporate the possibility of coherent back transfer.[17] Following this approach, we investigated the combined consequences of optical and spatial coherences in upconversion within the interacting pair system shown schematically in Fig. 4. Analytic results showed that sustained pulsations are expected in the populations of excited states in the intermediate to strongly coupled regime as the result of coherent cooperative upconversion.

Cooperative upconversion results from the excited-state atom–atom interaction between (unsymmetrized) product states $|02\rangle$ and $|11\rangle$ in the pair manifold shown in Fig. 4. Interactions between other excited pair states such as $|01\rangle$ and $|10\rangle$ are prevalent in rare-earth systems too but give rise only to companion phenomena such as rapid energy migration between sites. Such processes do not contribute to upconversion and are neglected here. Also, we considered the system at first to be undriven. Incident light prepares the system at time $t = 0$ in the doubly excited pair state $|11\rangle$ but has zero intensity thereafter. Modifications of energy-transfer processes in the presence of radiation are considered in Subsection 2.D.

Excited-state dynamics may be calculated from the Liouville equation for the density matrix ρ, augmented by relaxation terms:

$$i\hbar \frac{d\rho}{dt} = [H, \rho] - i\hbar\gamma\rho . \tag{9}$$

The Hamiltonian is taken to be $H = H_0 + H_{int}$, where H_0 is the isolated ion Hamiltonian and H_{int} is the interaction between two coupled atoms. Typically, H_{int} arises from multipole–multipole or exchange interactions between electrons on adjacent atoms,[18] but its detailed form is not of concern from the point of view of basic dynamics. Relaxation terms represented globally by γ include population decay of each level i at the rate γ_i and dephasing of polarization on the ij transition at the rate $\gamma_{ij} = (\gamma_i + \gamma_j)/2$. Off-diagonal elements of H are written as state-specific coupling parameters multiplied by Planck's constant. This permits the strength of the ion–ion interaction, for instance, to be given as a characteristic frequency $i\hbar L = \langle 02|H_{int}|11\rangle$, thus avoiding the need to specify multipole–multipole interactions or accompanying phonon processes explicitly. When the energies of the initially uncoupled states $|11\rangle$ and $|02\rangle$ are degenerate, one finds their eigenvalues in the presence of interaction by diagonalizing the subdeterminant of matrix elements of H. For example, with the pair basis shown in Fig. 4, the eigenvalues of submatrix

$$H = \begin{bmatrix} E & -i\hbar L^* \\ i\hbar L & E \end{bmatrix} \tag{10}$$

are readily found in the subspace of states $|11\rangle$ and $|02\rangle$ to be

$$E_{1,2}' = E \pm \hbar(LL^*)^{1/2} , \tag{11}$$

revealing an energy splitting of the doubly excited eigenstates equal to $2\hbar(LL^*)^{1/2}$. This is the well-known Davydov splitting. The corresponding eigenstates of the interacting pair are

$$\Psi_1 = \frac{|11\rangle - |02\rangle}{\sqrt{2}}, \qquad \Psi_2 = \frac{|11\rangle + |02\rangle}{\sqrt{2}} . \tag{12}$$

We examined the temporal development of superposition states rather than stationary states. States such as $|00\rangle$, $|11\rangle$, and $|02\rangle$ are spatially localized, and their dynamics directly reveal the spatial flow of energy within the system. This feature is extremely useful for understanding and predicting the energetics of the system. Because these states furnish a complete, alternative basis for describing pair dynamics in which intuitive ideas are easily incorporated, all the calculations were performed with them.

Introducing the convenient notation $|00\rangle = |0\rangle$, $|11\rangle = |1\rangle$, and $|02\rangle = |2\rangle$, one can immediately write equations of motion for the pair superposition states in the absence of driving fields as follows. Assuming the Davydov splitting is energetically negligible, one finds that

$$\frac{d\rho_{11}}{dt} = L\rho_{21} + L^*\rho_{12} - \gamma_1\rho_{11} , \tag{13}$$

$$\frac{d\rho_{22}}{dt} = (L\rho_{21} + L^*\rho_{12}) - \gamma_2\rho_{22} , \tag{14}$$

$$\frac{d\rho_{12}}{dt} = L(\rho_{22} - \rho_{11}) - \gamma_{12}\rho_{12} . \tag{15}$$

The analytic, steady-state solutions are

$$\rho_{11}(t) = \exp(-\gamma_{12}t)\left(\frac{2LL^*}{\omega_0^2} - \frac{\Delta^2 - \omega_0^2}{2\omega_0^2}\cos\omega_0 t - \frac{\Delta}{\omega_0}\sin\omega_0 t\right), \tag{16}$$

$$\rho_{22}(t) = \exp(-\gamma_{12}t)\left(\frac{2LL^*}{\omega_0^2}\right)(1 - \cos\omega_0 t) , \tag{17}$$

$$\rho_{12}(t) = \exp(-\gamma_{12}t)\left(\frac{2LL^*}{\omega_0^2}\right)[\Delta(1 - \cos\omega_0 t) - \omega_0 \sin\omega_0 t] . \tag{18}$$

In these expressions we have used the following definitions:

$$\Delta = (\gamma_1 - \gamma_2)/2, \tag{19}$$

$$\omega_0 = (4LL^* - \Delta^2)^{1/2}, \tag{20}$$

$$\rho_{12}'(t) = L\rho_{21} + L^*\rho_{12}. \tag{21}$$

Figure 5 shows the general behavior of these solutions for assumed initial conditions $\rho_{11} = 1$, $\rho_{22} = 0$, and $\rho_{12}' = 0$. The values of key parameters approximate those of Tm^{3+} in the crystal host $YAlO_3$, for which relevant relaxation rates are available in the literature.[19] Two values of the unknown coupling strength L were considered. For $L = 3$ kHz (three times the assumed dephasing rate), pulsations in the populations of pair superposition states $|1\rangle$ and $|2\rangle$ appeared as sinusoidal variations of ρ_{11} and ρ_{22} versus time. For $L = 1$ kHz (equal to the dephasing rate), no oscillations in population were predicted.

The population pulsations shown in Fig. 5(a) arise from periodic reversal of the cooperative upconversion process, a manifestation of (spatially coherent) partial delocalization of the excitation. Theoretically, the oscillation frequency provides a direct measure of the coupling strength L through the relation for ω_0 given in Eq. (20). At present this parameter may be estimated only roughly from measured pair cross-relaxation rates. However, this procedure does yield a value $L = 1$ kHz, which coincides with the experimental dephasing rate of level $|1\rangle$ (corresponding to the $^3F_4$ level of Tm^{3+}) in $Tm{:}YAlO_3$.[19] Because the coupling and decay rates are the same, this estimate suggests that, experimentally, L may be at the critical value separating regimes of localized from coherently delocalized dynamics. In $Tm{:}YAlO_3$ or other rare-earth crystals effects of delocalization may therefore be observable without optical cavities. Weakly delocalized dynamics may even seed unstable behavior in the presence of gain, an idea explored in more detail in Subsection 2.C.

C. Instabilities in Cooperative Dynamics

Because upconversion is inherently a nonlinear process, it can in principle exhibit unstable behavior.[29] Instabilities in excited-state populations or chaos might therefore be expected to arise from interatomic coupling of atoms[21] in at least two ways. First, one can imagine cooperative upconversion initiating population relaxation oscillations of the type indicated in Fig. 3, which might be amplified or sustained in the steady state by a driving field in a cavity. In this case oscillations would arise from cavity–atom interactions accompanied by stimulated emission. Second, the delocalization discussed in Subsection 2.B could initiate population pulsations and might be strong enough to mediate an instability even without a cavity. In this case unstable behavior would arise purely from atom–atom interactions driven by an optical field, without stimulated emission. In this subsection we find the surprising result that coherent delocalization is necessary to sustain steady-state oscillation with or without a cavity.

As an initial step, unstable solutions of the rate equations (4)–(8) were sought. Three-level lasers with linear driving terms respond universally to departures from steady-state intensity by exponential decay back to the original steady state.[22] However, upconversion is a nonlinear process, and a reexamination of this result in a multilevel pair system is warranted.

A linear stability analysis of Eqs. (4)–(8) was performed to investigate cooperative upconversion in a cavity in the limit of weak interatomic coupling. The steady-state population $(\rho_{ii})_{ss}$ for each excited state $|i\rangle$ was found for fixed intensity. Then linear departures from steady-state values were substituted into the dynamical equations through the replacement $\rho_{ii} \rightarrow (\rho_{ii})_{ss} + \Delta\rho_{ii}$. Eigenvalues of the equations of motion of $\Delta\rho_{ii}$ were then examined to determine whether deviations from steady-state values grew or decayed with time. This analysis (see Appendix A) revealed that populations always relax back to their steady-state values, with or without a cavity, for arbitrary values of incident intensity and decay constants. That is, rate equation analysis leads to the conclusion that pair-pumped upconversion lasers are universally stable.

In the intermediate-to-strong coupling regime a similar stability analysis of upconversion dynamics requires a density-matrix calculation. This begins with augmentation of the unperturbed Hamiltonian by the field Hamiltonian. In the basis of uncoupled pair states $|0\rangle$, $|1\rangle$, and $|2\rangle$ this yields

$$\hat{H}_0 = E|1\rangle\langle 1| + E|2\rangle\langle 2| + |\alpha|^2\hbar\omega|\alpha\rangle\langle\alpha|. \tag{22}$$

Here $|\alpha\rangle$ is a coherent state of the radiation field, chosen to represent the atomic interaction with a laser field,

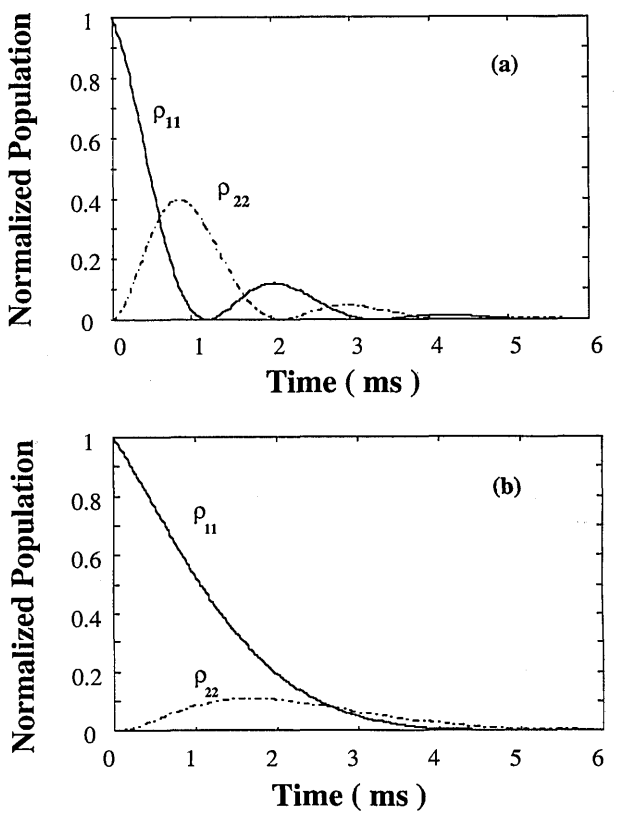

Fig. 5. Density-matrix calculation of excited pair state populations versus time in the presence of delocalization. The initial state is characterized by $\rho_{11} = 1$, $\rho_{22} = 0$, $\gamma_1 = \gamma_2 = 1$ kHz, and two values of interatomic coupling are considered, namely, (a) $L = 3$ kHz and (b) $L = 1$ kHz. Population pulsations are evident for the larger value of coupling.

and $|\alpha|^2 = \langle\alpha|a^\dagger a|\alpha\rangle$ is the expectation value of the number operator.[23] The energy contribution from vacuum fluctuations has been dropped. The ion–ion interaction Hamiltonian in this subspace is augmented by field-induced dipole transitions between the ground state $|0\rangle$ and the doubly excited pair state $|1\rangle$ (not state $|2\rangle$):

$$\hat{H}_{\text{int}} = i\hbar L|1\rangle\langle 2| + \text{h.c.} + \frac{\hbar f_A f_B{}^*|\alpha|^2}{\Delta\omega}|1\rangle\langle 0| + \text{h.c.} \quad (23)$$

In this expression $\Delta\omega$ is the $|00\rangle \rightarrow |01\rangle$ transition frequency, and h.c. denotes the Hermitian conjugate. The parameter f is the dipole moment on the $|0\rangle \rightarrow |1\rangle$ transition, defined by $f\alpha = \langle\mu \cdot E\rangle/\hbar$. Only the double-atom-excitation terms of interest have been retained from the second-order Hamiltonian $\langle 11|(\mu_A + \mu_B)\cdot E|01\rangle\langle 01|(\mu_A + \mu_B)\cdot E|00\rangle/\hbar\Delta\omega$. The subscripts A and B refer to atoms A and B of a coupled pair. Two-photon excitations of individual atoms have been specifically excluded from Eq. (23).

The populations of the pair system in the interaction representation are

$$\frac{d\rho_{00}}{dt} = \rho_3 + \gamma_1\rho_{11} + \gamma_2\rho_{22}, \quad (24)$$

$$\frac{d\rho_{11}}{dt} = \rho_3 + \rho_4 - \gamma_1\rho_{11}, \quad (25)$$

$$\frac{d\rho_{22}}{dt} = -\rho_4 - \gamma_2\rho_{22}. \quad (26)$$

The equations for optical and spatial coherences in the system are given by

$$\frac{d\rho_3}{dt} = I^2(\rho_{11} - \rho_{00}) - \gamma_{01}\rho_3, \quad (27)$$

$$\frac{d\rho_4}{dt} = 2\beta(\rho_{22} - \rho_{11}) - \gamma_{12}\rho_4, \quad (28)$$

respectively. Here γ_{01} and γ_{12} are the optical- and the spatial-coherence dephasing rates, and we have used the following definitions:

$$\rho_3 = (f\alpha)^2\rho_{10} + (f^*\alpha^*)^2\rho_{01}, \quad (29)$$

$$\rho_4 = -L(\rho_{12} + \rho_{21}), \quad (30)$$

$$I = 2|f|^2|\alpha|^2, \quad (31)$$

$$\beta = |L|^2. \quad (32)$$

We emphasize the role of incident light by replacing the expectation value of the number operator $\langle\alpha|n|\alpha\rangle = |\alpha|^2$ by a quantity I proportional to (but not identical with) intensity, as defined in Eq. (31).

In these equations the coherence term ρ_{02}, which is second order in the field, has been neglected. This at first appears unjustified because the coherence term ρ_{01}, which is similarly second order in the pumping field, has been retained. However, it can easily happen that sequential or simultaneous two-photon absorption processes fail to populate doubly excited states while cooperative upconversion takes place. If phonons accommodate the energy defect Δ, upconversion can occur rapidly and may generate weak spatial coherence or the delocalization described by ρ_{01}. At the same time, if energy levels are not in exact coincidence with the incident frequency, two-photon optical coherence does not develop ($\rho_{02} = 0$).

In a closed three-level pair system, population is conserved. Hence we can eliminate ground-state variables, using the relation $\rho_{00} + \rho_{11} + \rho_{22} = 1$. Making the substitutions $\rho_{11} \rightarrow \rho_1$ and $\rho_{22} \rightarrow \rho_2$ for convenience, we find that the equations of motion in matrix form become

$$\begin{bmatrix}\dot{\rho}_1\\ \dot{\rho}_2\\ \dot{\rho}_3\\ \dot{\rho}_4\end{bmatrix} = \begin{bmatrix}-\gamma_1 & 0 & 1 & -1\\ 0 & -\gamma_2 & 0 & -1\\ 2I^2 & I^2 & -\gamma_{01} & 0\\ -2\beta & 2\beta & 0 & -\gamma_{12}\end{bmatrix}\begin{bmatrix}\rho_1\\ \rho_2\\ \rho_3\\ \rho_4\end{bmatrix} + \begin{bmatrix}0\\ 0\\ I^2\\ 0\end{bmatrix}. \quad (33)$$

The overdots indicate differentiation with respect to time. The secular equation, of the general form $\lambda^4 + a_3\lambda^3 + a_2\lambda^2 + a_1\lambda + a_0 = 0$, has particularly simple coefficients if level $|1\rangle$ is assumed to be metastable ($\gamma_1 = 0$). Then the secular determinant factors into a trivial solution with zero eigenvalue and a cubic equation that can be solved analytically. Here we are interested only in identifying a condition that renders the real part of any eigenvalue positive because then the system will oscillate continuously. The Routh–Hurwitz criterion[24] for such an instability is that the system determinant $D = a_1a_2a_3 - a_{12} - a_0a_{32} = \beta\gamma_2{}^2(16\beta + 3\gamma_2{}^2 - 3I)/2$ must be zero or negative. This condition occurs when the intensity I exceeds the critical value

$$I_c = \left(\frac{16\beta + 3\gamma_2{}^2}{3}\right)^{1/2}. \quad (34)$$

From this result it may be concluded that spatial coherence can generate population oscillations in the steady state without optical feedback. This feature of coherent cooperative upconversion has not, to our knowledge, been previously discussed and may be a useful new signature of delocalization in upconversion. A numerical calculation of the growth of this instability is shown in Fig. 6.

D. Enhanced Upconversion and Energy Transfer

We now show that the energy-transfer rate between atoms is frequency dependent when modulated, incoherent light is used to excite pair upconversion. A resonant condition for enhanced upconversion emerges from this analysis.

The dynamical equations that we consider are identical to Eqs. (13)–(15), except that an incoherent driving term is added to the right-hand side of Eq. (14). The modified equation is

$$\frac{d\rho_{22}}{dt} = -(L\rho_{21} + L^*\rho_{12}) - \gamma_2\rho_{22} + \lambda_p. \quad (35)$$

The optical pumping rate λ_p depends on incident intensity, the Einstein B coefficient, and the population difference between levels $|0\rangle$ and $|1\rangle$. In the low-depletion limit $\rho_{00} - \rho_{11} \cong 1$, and λ_p is implicitly independent of the density-matrix elements. Writing the equations of motion in terms of ρ_{12}' defined in Eq. (20), we find that

$$\begin{bmatrix}\dot{\rho}_{11}\\ \dot{\rho}_{22}\\ \dot{\rho}_{12}'\end{bmatrix} = \begin{bmatrix}-\gamma_1 & 0 & 1\\ 0 & -\gamma_2 & -1\\ -2\beta & 2\beta & -\gamma_{12}\end{bmatrix}\begin{bmatrix}\rho_{11}\\ \rho_{22}\\ \rho_{12}'\end{bmatrix} + \begin{bmatrix}0\\ \lambda_p(t)\\ 0\end{bmatrix}. \quad (36)$$

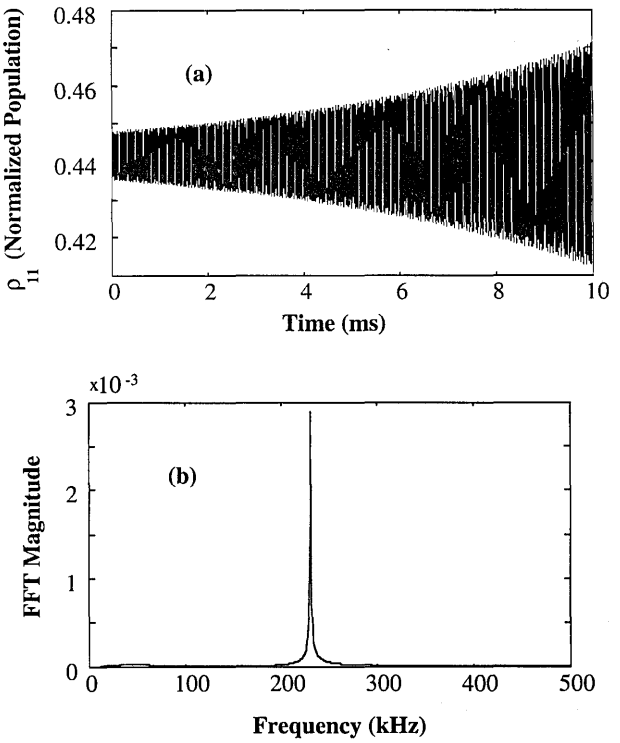

Fig. 6. Growth of quasi-periodic output from a constant steady-state condition of a pair-pumped laser (density-matrix calculation). (a) $l^2 = 2.6 \times 10^4$ kHz^2, $\beta = 900$ kHz^2, and $\gamma_2 = 100$ cm^{-1}, $\gamma_1 = 0$. (b) Fourier spectrum of (a).

If the incident field is modulated at a frequency ω according to $\lambda_p(t) = \lambda_p(0)\exp(i\omega t)$, then harmonic solutions exist of the form

$$\begin{bmatrix} \rho_{11}(t) \\ \rho_{22}(t) \\ \rho_{12}'(t) \end{bmatrix} = \begin{bmatrix} \rho_{11}(0) \\ \rho_{22}(0) \\ \rho_{12}'(0) \end{bmatrix} \exp(i\omega t), \tag{37}$$

and substitution into Eq. (36) yields the solutions given by

$$\rho_{11}(0) = \frac{(\gamma_2 + i\omega)(\gamma_{12} i\omega) + 2\beta}{(\gamma_{12} + i\omega)[(\gamma_{12} + i\omega)^2 + \omega_0{}^2]} \lambda_p(0), \tag{38}$$

$$\rho_{22}(0) = \frac{2\beta}{(\gamma_{12} + i\omega)[(\gamma_{12} + i\omega)^2 + \omega_0{}^2]} \lambda_p(0), \tag{39}$$

$$\rho_{12}'(0) = \frac{-2\beta(\gamma_2 + i\omega)}{(\gamma_{12} + i\omega)[(\gamma_{12} + i\omega)^2 + \omega_0{}^2]} \lambda_p(0). \tag{40}$$

In these expressions a resonant frequency ω_0 appears, defined by

$$\omega_0 = \left[4\beta - \left(\frac{\gamma_1 - \gamma_2}{2} \right)^2 \right]^{1/2}. \tag{41}$$

The physical meaning of Eqs. (38)–(40) can best be appreciated by comparison of the fluorescence intensity at a particular frequency with that at zero frequency ($\omega = 0$), with a response function defined by

$$R(\omega) = \left| \frac{\rho_{22}(0)}{\rho_{22}(0)|_{\omega=0}} \right| = \frac{\gamma_{12}(\gamma_{12}{}^2 + \omega_0{}^2)}{\{(\omega_0{}^2 + \gamma_{12}{}^2)[(\omega_0{}^2 - \omega^2 + \gamma_{12}{}^2)^2 + 4\omega^2\gamma_{12}{}^2\}^{1/2}}. \tag{42}$$

$R(\omega)$ is proportional to emission intensity, which is dependent on energy transfer, and is plotted in Fig. 7 for two values of the interatomic coupling strength L, again with the use of decay parameters typical of Tm:$YAlO_3$. For weak coupling ($L = 0.5$ kHz), the energy-transfer response function falls off rapidly as the frequency of modulation is increased from zero. However, for stronger coupling ($L = 5$ kHz) it exhibits a resonant peak near the coupling frequency. The precise frequency at which the peak occurs is given by

$$\omega_{\max}^2 = \frac{3\omega_0{}^2 - 4\gamma_{12}{}^2 + (\omega_0{}^2 - 32\omega_0{}^2\gamma_{12}{}^2)^{1/2}}{4}. \tag{43}$$

When the dephasing rate of spatial coherence is much less than the coupling frequency, the energy-transfer resonance is well defined. When the dephasing rate exceeds the coupling frequency, the peak broadens and becomes less pronounced, eventually disappearing.

3. EXPERIMENTAL PROCEDURES

To investigate some of these predictions, experiments were performed in single crystals of 5% Er:CaF_2 and 5% Er:$LiYF_4$. Two sample disks of 3-mm thickness were prepared as monolithic, hemispherical optical cavities, and a third sample of the same thickness was polished plane parallel. The monolithic crystals were cut and were polished identically for laser experiments, with one flat surface and one convex surface of radius 2.5 cm. Both surfaces were antireflection coated in the range 1.4–1.6 μm. Most observations were made in the first

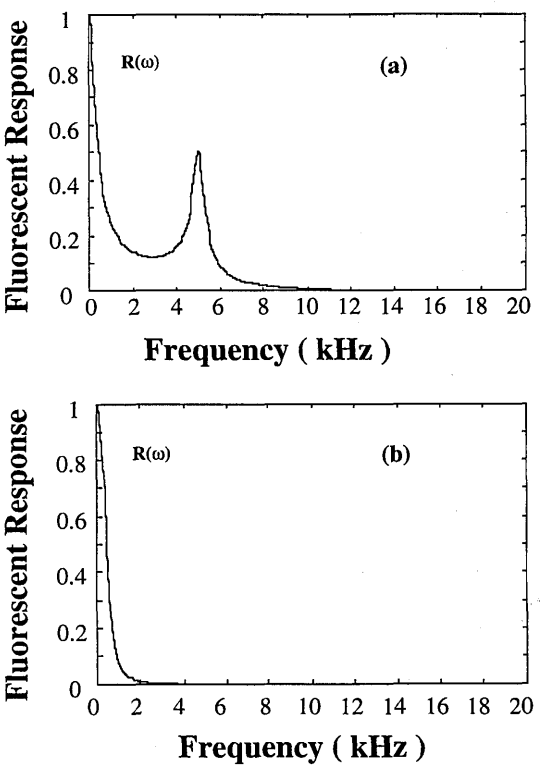

Fig. 7. Response function for enhanced energy transfer resulting from modulation of the optical driving field for two values of the interatomic coupling strength L. (a) $L = 5$ kHz, (b) $L = 0.5$ kHz. Other parameters used are $\gamma_1 = 0.43$ kHz (twice the measured[19] decay rate), $\gamma_2 = 1.6$ kHz, and $\gamma_{12} = 1.02$ kHz.

crystal, in which the curved surface coating gave total reflection between 2.7 and 2.9 μm and the flat served as a 2% output coupler. The other monolithic sample was coated for output at 854 nm. The third sample was used in an astigmatically compensated, three-mirror cavity designed for operation at 702 nm. Collectively these samples furnished light sources in which emission was sustained by pair, trio, and quartet upconversion processes, respectively.

Each sample was pumped longitudinally with a cw NaCl color-center laser, absorbing approximately 75% of incident radiation at 1.51 μm. Laser action at 2.8 μm was achieved at room temperature, as described previously.[14] The lasers with output wavelengths at 855 (Ref. 25) and 702 nm (Ref. 26) required cooling to liquid-nitrogen and liquid-helium temperatures, respectively. Cw laser emission was observed in each sample with output powers in the milliwatt range, sufficient for a variety of experiments related to cooperative dynamics. Laser output of the first crystal was monitored through a notch filter at 2.8 μm (FWHM 10 nm) with a fast InAs photodiode (rise time ~5 ns). Dynamics at 854 and 702 nm were monitored with fast photomultipliers and were recorded on a 1-GHz digital oscilloscope. Thermopile detection was used for power measurements.

Two main types of time-resolved measurement pertinent to a comparison with the theoretical concept outlined in Section 2 were made. The first consisted of observations of 2.8-μm laser output transients at the leading and trailing edges of square pump pulses generated by acousto-optic techniques. We made single-shot digital recordings with 100-ns temporal resolution (analog bandwidth), using a 1-MHz sampling rate over 8,000 points. Second, output intensity was digitally recorded versus time in the instability regime, with constant pumping.

4. RESULTS AND DISCUSSION

A. Enhanced Quantum Efficiency

The most efficient upconversion laser in our experiments was the unoptimized trio laser, which operated at 855 μm. Measurements yielded a slope efficiency of 28% and an overall energy efficiency of 26% for this laser. The latter value is to be compared with the maximum theoretical limits with and without recycling, which give $\eta_E{}^* = [1/(m-1)]\lambda_{in}/\lambda_{out} = 88\%$ and $\eta_E = (1/m)\lambda_{in}/\lambda_{out} = 59\%$, respectively. Although the cw trio laser worked remarkably well on a self-terminating transition, the actual laser efficiency gave no indication of quantum-efficiency enhancement.

Figure 8 shows representative data for upconversion laser emission on the $^2H_{9/2}$–$^4I_{11/2}$ transition at 701.5 nm, excited by 1.5-μm radiation and originating from a state at nearly four times the incident photon energy. The mere operation of this fourfold upconversion laser is surprising and immediately raises questions as to what fundamental limits may exist for cw laser action involving high degrees of upconversion and whether enhancement mechanisms are operative in such devices. However, the fourfold upconversion laser was also less efficient than either the maximum value $\eta_E{}^* = 71\%$ or $\eta_E = 53\%$. Consequently it was not possible to conclude directly from these laser measurements whether cooperative enhancement affected performance.

Nevertheless, other recent observations support the concept of cooperatively enhanced quantum efficiency outlined in Subsection 2.A. Output power measurements of a 2.8-μm laser pumped by conventional means at 980 nm in concentrated Er:$LiYF_4$ recently revealed performance marginally in excess of the theoretical efficiency limit set by $\eta_E = \lambda_{in}/\lambda_{out} \cong 35\%$.[27] This result was ascribed to pair upconversion dynamics, furnishing the first example of a laser with output enhanced by cooperative dynamics. Enhancement should extend to cooperative upconversion lasers as well, however. Although our own measurements do not reveal enhancement of upconversion laser output, we do furnish direct evidence of recycling dynamics in Subsection 4.B.

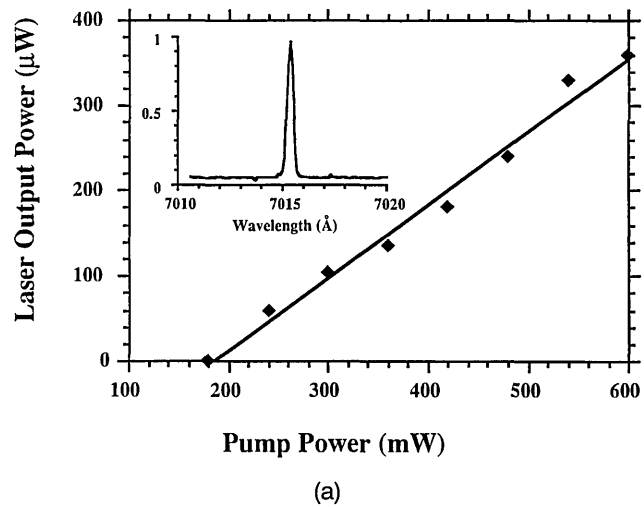

(a)

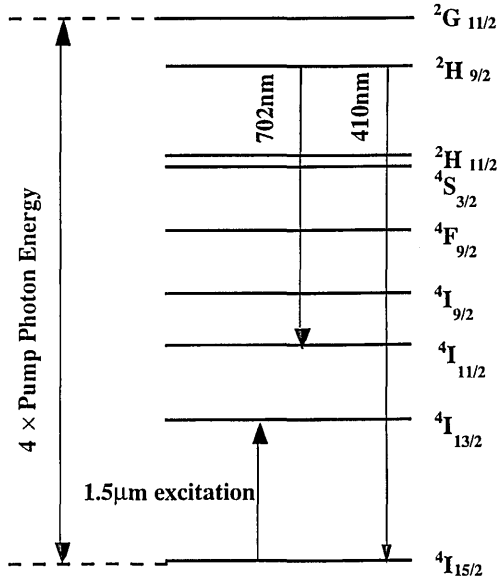

(b)

Fig. 8. Output versus input power for the fourfold cw upconversion laser operating at 701.5 nm (λ_{ex} = 1.5 μm). Inset, laser emission spectrum. (b) Energy diagram identifying the Er^{3+} levels involved in the pumping and the emission processes of the fourfold upconversion laser.

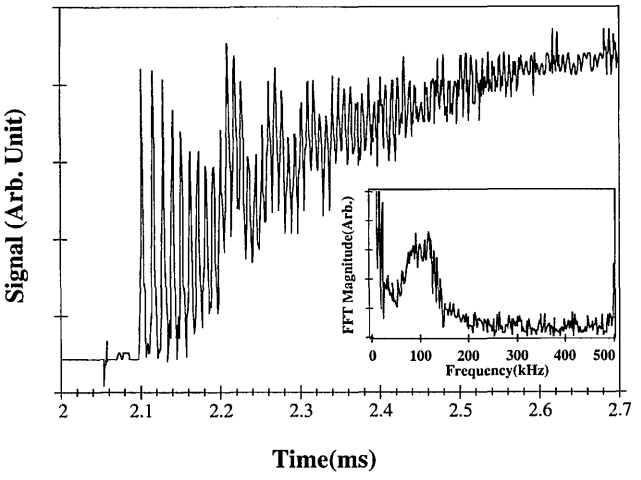

(a)

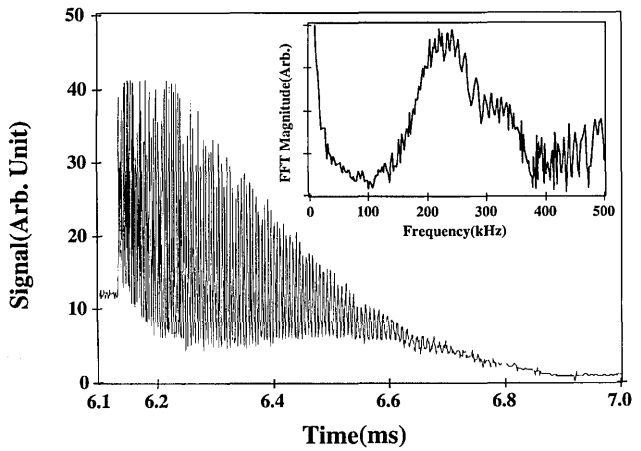

(b)

Fig. 9. Oscillations in output power observed at (a) the leading and (b) the trailing edges of a 2.8-μm Er:$LiYF_4$ laser pulse excited by a square pulse at $\lambda_{ex} = 1.5$ μm of 10-ms duration. Excitation was gated acousto-optically from the output of a cw NaCl laser. The rise and fall times of the pump pulses were less than 50 ns. Insets, Fourier transforms showing dominant frequency components.

B. Population Pulsations

When cw operation of the 2.8-μm pair-pumped laser was terminated, a transient increase in output power was observed. This result is in accord with the simple rate equation treatment presented in Subsection 2.B. In addition, for excitation at $\lambda_{ex} = 1.5$ μm, unexpected rapid oscillations occurred under the envelope of this transient peak, as shown in Fig. 9. Relaxation oscillations were observed at the leading edge of pump pulses also [Fig. 9(a)] but are not discussed here because of the analytic complication of including a driving field in the dynamics. Conclusions may be drawn more straightforwardly from an examination of trailing-edge transients.

An enlargement of postexcitation pulsations is shown in Fig. 9(b), together with their Fourier spectrum, revealing a chirped frequency spectrum centered near 210 kHz. This frequency is very near the measured inverse lifetime $(1/\pi\tau) = 210$ kHz of the $^4I_{9/2}$ level of Er^{3+}:$LiYF_4$. From Fig. 9(b) it is clear that pulsations of the stimulated emission continued long after external excitation of the system ceased. This clearly indicates that they originate from the interaction of the residual atomic inversion, the optical cavity, and the cavity photon density. Moreover, these pulsations are in excellent quantitative agreement with the rate equation calculation given in Fig. 3, with no adjustable parameters.

The origin of these transient pulsations can be pictured in the following way. Once external excitation ceases, inversion can recur only through pair upconversion to the $^4I_{9/2}$ level (analogous to level $|3\rangle$ in Fig. 2) of Er^{3+}. This process[14] is followed by nonradiative relaxation to the $^4I_{11/2}$ upper laser level ($|2\rangle$ in Fig. 2). While the upconversion rate is very high, the limiting rate at which inversion can be reestablished following depletion of the gain is set by the inverse $^4I_{9/2}$ lifetime. As long as the $^4I_{13/2}$ level ($|1\rangle$ in Fig. 2) responsible for pair upconversion remains well populated, cooperative upconversion efficiently replenishes the upper-state population in this way. Inversion density builds until the threshold is reached, whereupon stimulated emission depletes the accumulated gain. Quite distinct from conventional relaxation oscillations, these population pulsations are a direct manifestation of population recycling by cooperative dynamics, amplified by the feedback within an optical cavity.

C. Instabilities in Driven Systems

Whereas true cw operation of the pair-pumped 2.8-μm laser was achieved at low pumping intensity, instabilities became evident at intensities well above the threshold for cw lasing. These results are shown in Figs. 10–12.

For an excitation wavelength of $\lambda_{ex} = 1.5$ μm, inversion at 2.8 μm is sustained purely by cooperative dynamics.[14]

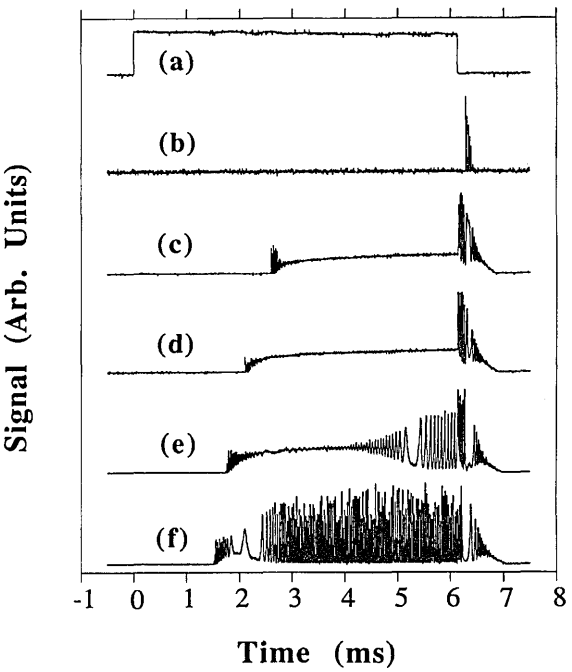

Fig. 10. Traces of pair-pumped Er:CaF_2 laser output at 2.8 μm at various pumping intensities. (a) The pump pulse. (b) Threshold operation. (c) True cw operation with leading- and trailing-edge transients (1.1 times threshold). (d) Cw operation at higher power (1.5 times threshold). (e) The growth of sustained oscillation from noise (two times threshold). (f) Unstable, quasi-periodic output (three times threshold).

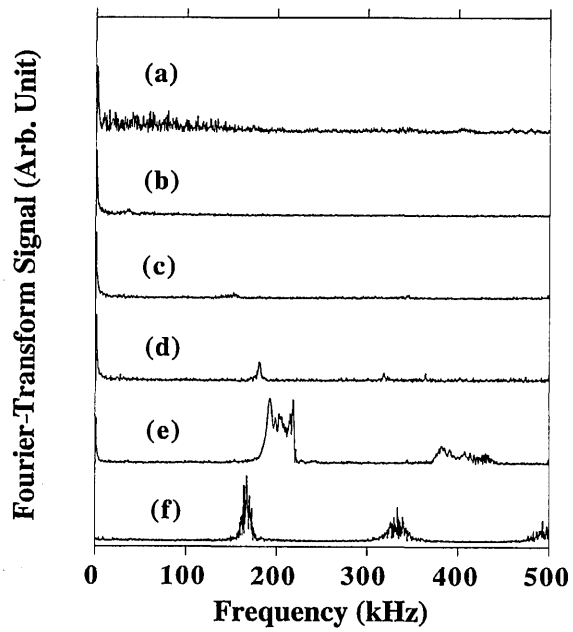

Fig. 11. Fourier transforms of the Fig. 10 time series, showing the presence of several modulation frequencies at high pumping intensity but no subharmonics. Leading- and trailing-edge transients were excluded from the analysis.

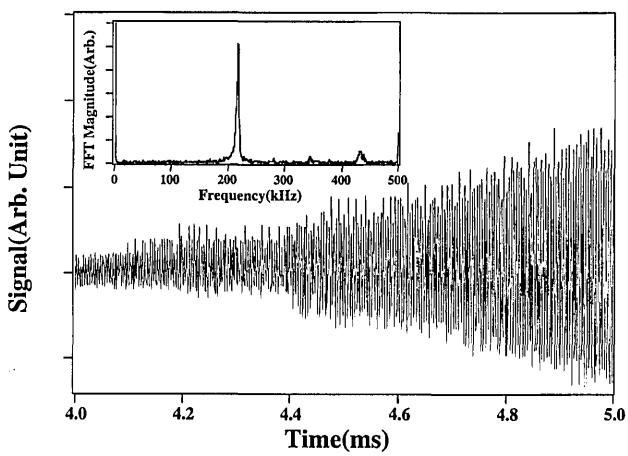

Fig. 12. Experimental trace of the growth of the instability shown in Fig. 10(e) with high temporal resolution. Inset, Fourier-transform spectrum.

At other excitation wavelengths the cooperative process occurs at a much reduced rate because the steady-state $^4I_{13/2}$ population from which pair upconversion originates is greatly reduced. The main result of this section is that instabilities are observed only when the excitation wavelength is chosen to maximize the cooperative dynamic contribution to laser inversion ($\lambda_{ex} = 1.5\ \mu m$).

The experimental observation of spontaneous growth of an instability from noise above a distinct threshold intensity is shown in Fig. 10. The associated Fourier spectrum is presented in Fig. 11, and a second recording is shown in Fig. 12, with higher temporal resolution. These experimental results are in excellent agreement with the density-matrix prediction given in Fig. 6. At this pumping intensity laser output experiences a hard loss of stability characteristic of a subcritical Hopf bifurcation,[28] suddenly developing a deep, periodic modulation above the instability threshold. Oscillations grow progressively more complex as pumping is increased, possibly because of a secondary Hopf bifurcation on a torus.

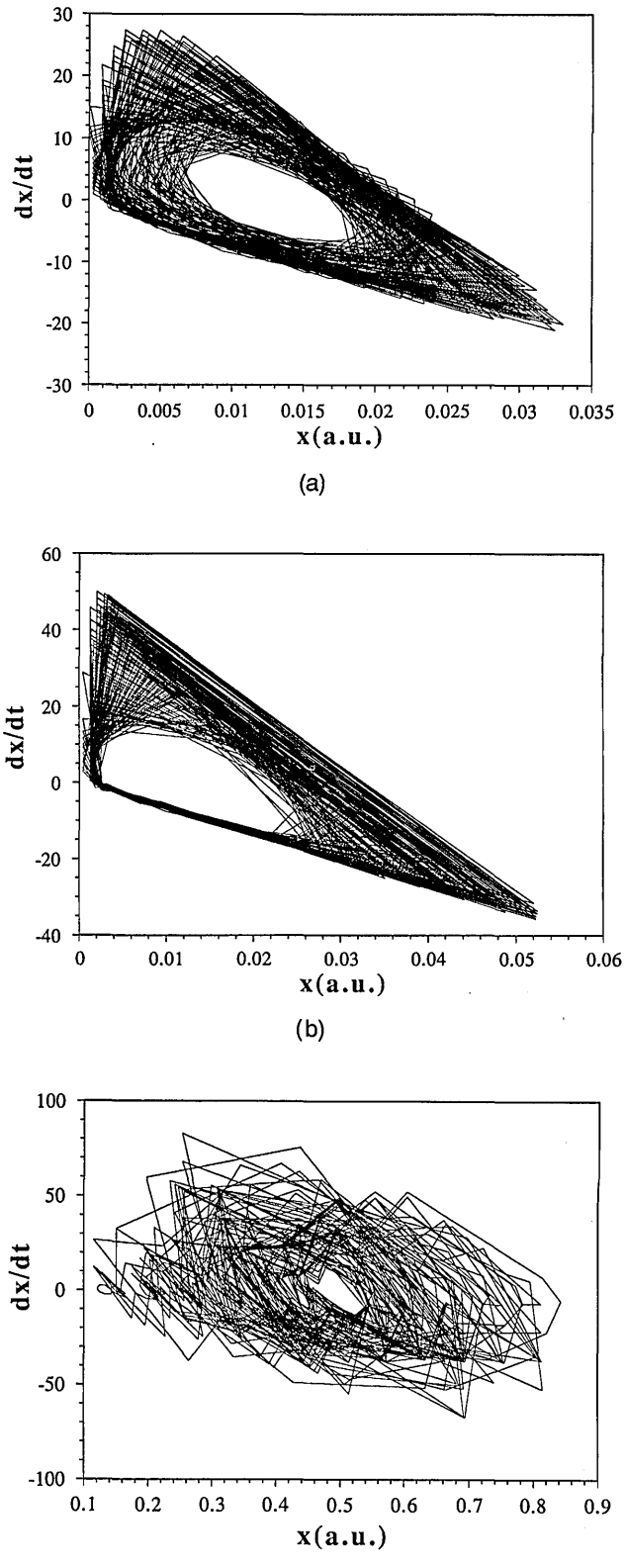

Fig. 13. Phase space plots of unstable output from the 2.8-μm pair-pumped laser: (a) dx/dt versus t for the $x(t)$ time sequence in the 3–6-ms interval shown in Fig. 10(e) at two times laser threshold ($Er:CaF_2$), (b) dx/dt versus t at three times laser threshold ($Er:CaF_2$), (c) dx/dt versus t at five times laser threshold ($Er:LiYF_4$).

This progression is reflected in the attractor plots shown in Fig. 13.

Although the 2.8-μm laser is renowned for being noisier than most other solid-state lasers under free-running conditions, to our knowledge no sustained oscillations like those reported here have been observed for excitation at pump wavelengths other than 1.5 μm. In our experiments, in addition to using $\lambda_{ex} = 1.5$ μm to pump 2.8-μm Er:CaF_2 and Er:$LiYF_4$ lasers, we tried alternative wavelengths of $\lambda_{ex} = 651-657$ nm and $\lambda_{ex} = 800$ nm. As indicated in Fig. 14, the output observed from the 2.8-μm Er:CaF_2 laser pumped three times over threshold at $\lambda_{ex} = 652$ nm showed no spiking behavior during continuous operation. After termination of pumping at $\lambda_{ex} = 652$ nm this laser showed transient enhancement of laser output (an afterpulse), but population pulsations beneath the afterpulse envelope were notably absent. Similarly, for $\lambda_{ex} = 800$ nm, no sustained oscillations were observed at equivalent levels above threshold, and no postexcitation pulsations occurred.

At pump wavelengths other than 1.5 μm, cooperative dynamics evidently served to overcome the self-terminating nature of the 2.8-μm emission but contributed only weakly to upper-laser-level population. Oscillations in 2.8-μm laser emission did not occur under these circumstances. Unstable operating conditions were reached only when excitation was provided at 1.5 μm, for only then did nonlinear cooperative dynamics dominate the inversion mechanism. We take these results, in combination with the theoretical considerations of Subsections 2.B and 2.C, to be strong evidence that the observed instabilities of the pair-pumped laser are completely attributable to cooperative nonlinear dynamics. Additionally, one may infer that noisy operation of the 2.8-μm Er laser pumped at wavelengths other than 1.5 μm originates from a subthreshold instability of the cooperative upconversion contribution to gain in the laser medium. Improved operation of this laser might therefore be attainable with feedback control of the type recently applied to stabilize chaotic laser output.[29]

5. SUMMARY

Cooperative nonlinear dynamics in highly doped media have important implications for upconversion and conventional solid-state lasers alike. In this paper we have introduced the concepts of population recycling in cooperative upconversion and enhancement of quantum efficiency. These concepts are relevant to an understanding of the theoretical efficiency limits of cw upconversion lasers and to potential improvements of conventional lasers in dense media.

Cooperative dynamics give rise to population pulsations and instabilities that can be observed in optical cavities. We have established that pulsations during afterpulses and sustained oscillations of the cw pair-pumped Er laser operating at 2.8 μm are due to the nonlinear dynamics of cooperative upconversion and can be reproduced by a density-matrix theory of cooperative upconversion that incorporates spatial coherence. Rate equations successfully describe transient upconversion behavior but fail to reproduce the observed steady-state instabilities, thereby indicating the importance of spatial coherence in pair dynamics of rare-earth ions in upconversion lasers. Coherent cooperative upconversion can in principle mediate population pulsations in rare-earth systems without cavities and admits a measure of control over energy transfer. These interesting prospects warrant further investigation.

APPENDIX A

To analyze the stability of the pair-pumped upconversion laser, the system response to small perturbations in Eqs. (4)–(8) must be examined. Solutions of the excited-state populations that grow with time are sought after one writes the time-dependent population $N_i(t)$ of level $|i\rangle$ as a sum of its steady-state value N_{is} and its fluctuation n_i, according to $N(t) = N_{is} + n_i$. Similarly, $Q(t) = Q_s + q$, and it is assumed that $n_i/N_{is} \ll 1$ and $q/Q_s \ll 1$.

Using $n_0 + n_1 + n_2 + n_3 = 0$, one obtains the following reduced set of dynamical equations for the fluctuations themselves:

$$\begin{bmatrix} \dot{n}_0 \\ \dot{n}_1 \\ \dot{n}_2 \\ \dot{q} \end{bmatrix} = \begin{bmatrix} -B_{01}I - \gamma_{30} & B_{01}I + 2\alpha N_{1s}\gamma_1 - \gamma_{30} & \gamma_{20} - \gamma_{30} & 0 \\ B_{01}I - \gamma_{31} & -B_{01}I - B_{12}Q_s - 4\alpha N_{1s} - \gamma_1 - \gamma_{31} & [B_{12}Q_s + \gamma_{21} - \gamma_{31}] & B_{12}(N_{2s} - N_{1s}) \\ -\gamma_{32} & B_{12}Q_s - \gamma_{32} & -B_{12}Q_s - \gamma_2 - \gamma_{32} & -B_{12}(N_{2s} - N_{1s}) \\ 0 & -B_{12}Q_s & B_{12}Q_s & 0 \end{bmatrix} \begin{bmatrix} n_0 \\ n_1 \\ n_2 \\ q \end{bmatrix}. \quad \text{(A1)}$$

Solutions of Eq. (A1) exist of the form

$$\begin{bmatrix} n_0(t) \\ n_1(t) \\ n_2(t) \\ q(t) \end{bmatrix} = \begin{bmatrix} n_0(t) \\ n_1(t) \\ n_2(t) \\ q(t) \end{bmatrix} \exp(\lambda t), \quad \text{(A2)}$$

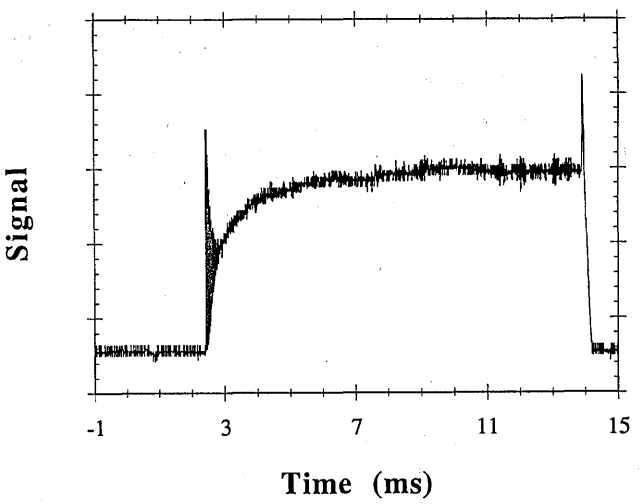

Fig. 14. Output trace of the 2.8-μm Er:CaF_2 laser pumped by a long square pulse in the red spectral region ($\lambda_{ex} = 652$ nm). At this pump wavelength output is continuous even at three times above threshold, and the trailing-edge spike has no rapid underlying oscillations.

where λ is an eigenvalue of the matrix $\mathbf{A}$ of coefficients in Eq. (A1). Eigenvalues are determined by setting $\mathrm{Det}[\mathbf{A} - \lambda U] = 0$, where U is the unit tensor, and this secular equation can be written in the form $a_4\lambda^4 + a_3\lambda^3 + a_2\lambda^2 + a_1\lambda + a_0 = 0$. The coefficients a_i are determined by explicit evaluation of the secular determinant. The system becomes unstable if any root is positive, for then the small initial perturbation will grow exponentially in time according to Eq. (A2).

The Routh–Hurwitz criterion[24] for stability requires an examination of the following determinants:

$$D_1 = a_1, \qquad D_2 = \begin{vmatrix} a_1 & a_0 \\ a_3 & a_2 \end{vmatrix}, \qquad D_3 = \begin{vmatrix} a_1 & a_0 & 0 \\ a_3 & a_2 & a_1 \\ 0 & a_4 & a_3 \end{vmatrix},$$

$$D_4 = \begin{vmatrix} a_1 & a_0 & 0 & 0 \\ a_3 & a_2 & a_1 & 0 \\ 0 & a_4 & a_3 & a_2 \\ 0 & 0 & 0 & a_4 \end{vmatrix}. \tag{A3}$$

The coefficients are

$$\begin{aligned} a_0 &= abcd + \gamma_3[3abd + bcd + bd(\gamma_{10} + \gamma_{20})] + bcd\gamma_{30}, \\ a_1 &= abc + 3abd + 2bcd + bd(2\gamma_3 + \gamma_{20} + \gamma_{10}) \\ &\quad + 3ab\gamma_3 + ac(\gamma_2 + \gamma_{32}) + bc(\gamma_3 + \gamma_{30}) + 2a\gamma_2\gamma_3 \\ &\quad + b\gamma_3(\gamma_{10} + \gamma_{20}) + c(\gamma_2\gamma_{30} + \gamma_2\gamma_3 + \gamma_{20}\gamma_{32}) \\ &\quad + \gamma_{10}\gamma_2\gamma_3, \\ a_2 &= ac + 3ab + 2bc + 2bd + 2a(\gamma_2 + \gamma_3) \\ &\quad + b(\gamma_{10} + \gamma_{20} + 2\gamma_3) + c(2\gamma_2 - 2\gamma_{30} + \gamma_{31} + 2\gamma_{32}) \\ &\quad + [\gamma_{10}(\gamma_2 + \gamma_3) + \gamma_2\gamma_3], \\ a_3 &= 2(a + b + c) + \gamma_1 + \gamma_2 + \gamma_3, \\ a_4 &= 1. \end{aligned} \tag{A4}$$

Here we have used the definitions $a = B_{01}l$, $b = B_{12}Q_s$, $c = 2aN_{1s}$, and $d = B_{12}(N_{2s} - N_{1s}) = t_c^{-1}$, and we note that all these quantities and the coefficients given above are positive above laser threshold. The system will become unstable if any determinant $D_1(i = 1, 2, 3, 4)$ is less than zero.

Because $a_4 = 1$ we note that $D_4 = D_3$, so the number of determinants that must be considered is reduced to three:

$$D_1 = a_1, \tag{A5}$$

$$D_2 = a_1a_2 - a_3a_0, \tag{A6}$$

$$D_3 = a_3D_2 - a_4{a_1}^2. \tag{A7}$$

From Eqs. (A4) it is evident that $a_i > 0$ for all i. Hence, for an instability to develop, it is necessary that either $D_2 < 0$ or $D_3 < 0$. However, one can easily verify, by expanding Eqs. (A6) and (A7) directly and by canceling all negative terms, that D_2 and D_3 are always positive for positive inversion $(N_{2s}-N_{1s})$. Consequently the rate equations describing pair-pumped laser operation are universally stable.

ACKNOWLEDGMENTS

The authors gratefully acknowledge research support by the U.S. Air Force Office of Scientific Research (H. Schlossberg) and thank S. Rai and J. Rai for useful discussions.

*Present address, Los Alamos National Laboratory, CLS-6 Group/MS E535, Los Alamos, New Mexico 87545.

REFERENCES AND NOTES

1. F. Auzel, Proc. IEEE **61,** 758 (1973).
2. S. Hufner, *Optical Spectra of Transparent Rare Earth Compounds* (Academic, New York, 1978), Chap. 5.
3. O. K. Alimov, M. Kh. Ashurov, T. T. Basiev, E. O. Kirpichenkova, and V. B. Murav'ev, in *Selective Laser Spectroscopy of Activated Crystals and Glasses,* V. V. Osiko, ed. (Nova Science, New York, 1988), Chap. 2.
4. J. Chivian, W. Case, and D. Eden, Appl. Phys. Lett. **35,** 124 (1979).
5. H. Ni and S. C. Rand, Opt. Lett. **16,** 1424 (1991).
6. A comprehensive review of upconversion processes is given by J. C. Wright, "Up-conversion and excited state energy transfer in rare-earth doped materials," in *Topics in Applied Physics,* F. K. Fong, ed. (Springer, New York, 1976), Vol. 15, p. 239.
7. R. M. Macfarlane, F. Tong, A. J. Silversmith, and W. Lenth, Appl. Phys. Lett. **52,** 1300 (1988).
8. R. J. Thrash and L. F. Johnson, J. Opt. Soc. Am. B **11,** 881 (1994).
9. J. Y. Allain, M. Monerie, and H. Poignant, Electron. Lett. **26,** 261 (1990).
10. R. G. Smart, D. C. Hanna, A. C. Tropper, S. T. Davey, S. F. Carter, D. Szebesta, Electron. Lett. **27,** 1307 (1991).
11. S. G. Grubb, K. W. Bennett, R. S. Cannon, and W. F. Humer, in *Conference on Lasers and Electro-Optics,* Vol. 12 of 1992 OSA Technical Digest Series (Optical Society of America, Washington, D.C., 1992), pp. 669–670.
12. D. S. Funk, S. B. Stevens, and J. G. Eden, IEEE Photon. Technol. Lett. **5,** 154 (1993).
13. P. Xie and S. C. Rand, Opt. Lett. **17,** 1116, 1822 (1992).
14. P. Xie and S. C. Rand, Opt. Lett. **15,** 848 (1990).
15. P. Xie, "Continuous-wave cooperative upconversion lasers," Ph.D. dissertation (University of Michigan, Ann Arbor, Mich., 1992).
16. H. Chou, "Upconversion processes and Cr-sensitization of Er- and Er, Ho-activated solid state laser materials," Ph.D. dissertation (Massachusetts Institute of Technology, Cambridge, Mass., 1989).
17. A. S. Davydov and A. A. Serikov, Phys. Status Solidi **51,** 57 (1972).
18. R. B. Barthem, R. Buisson, J. C. Vial, and H. Harmand, J. Lumin. **34,** 295 (1986).
19. L. M. Hobrock, "Spectra of thulium in yttrium orthoaluminate crystals and its four-level laser operation in the mid-infrared," Ph.D. dissertation (University of Southern California, Los Angeles, Calif., 1972). In the present paper we follow recent practice by exchanging the labels of the $^3H_4$ and the $^3F_4$ states of Tm with respect to Hobrock, designating $^3F_4$ as the first excited state. See, e.g., A. Brenier, J. Rubin, R. Moncorge, and C. Pedrini, J. Phys. (Paris) **50,** 1463 (1989).
20. See, e.g., R. Seydel, *From Equilibrium to Chaos* (Elsevier, New York, 1988).
21. J. Rai and C. M. Bowden, in *International Conference on Quantum Electronics,* Vol. 8 of 1990 OSA Technical Digest Series (Optical Society of America, Washington, D.C., 1990), paper QTuN3.
22. D. M. Sinnett, J. Appl. Phys. **33,** 1578 (1962).
23. R. Loudon, *The Quantum Theory of Light,* 2nd ed. (Clarendon, Oxford, 1983), pp. 146–152.
24. See, e.g., *Handbook of Mathematics,* I. N. Bronshtein and K. A. Semendyayev, eds. (Van Nostrand Reinhold, New York, 1985), p. 419.
25. P. Xie and S. C. Rand, Opt. Lett. **17,** 1198 (1992); **17,** 1822 (1992).
26. P. Xie and S. C. Rand, Appl. Phys. Lett. **63,** 3125 (1993).
27. R. C. Stoneman and L. Esterowitz, Opt. Lett. **17,** 816 (1992).
28. See, e.g., Ref. 20, p. 73.
29. Z. Gills, C. Iwata, R. Roy, I. B. Schwartz, and I. Triandaf, Phys. Rev. Lett. **69,** 3169 (1992).